Journal of Statistical Physics, Vol. 48, Nos. 3/4, 1987

Diffusion in a Periodic Lorentz Gas

Bill Moran,[1] William G. Hoover,[1] and Stronzo Bestiale[2]

Received January 21, 1987

We use a constant "driving force" F_d together with a Gaussian thermostatting "constraint force" F_c to simulate a nonequilibrium steady-state current (particle velocity) in a periodic, two-dimensional, classical Lorentz gas. The ratio of the average particle velocity to the driving force (field strength) is the Lorentz-gas conductivity. A regular "Galton-board" lattice of fixed particles is arranged in a dense triangular-lattice structure. The moving scatterer particle travels through the lattice at constant kinetic energy, making elastic hard-disk collisions with the fixed particles. At low field strengths the nonequilibrium conductivity is statistically indistinguishable from the equilibrium Green–Kubo estimate of Machta and Zwanzig. The low-field conductivity varies smoothly, but in a complicated way, with field strength. For moderate fields the conductivity generally decreases nearly linearly with field, but is nearly discontinuous at certain values where interesting stable cycles of collisions occur. As the field is increased, the phase-space probability density drops in apparent fractal dimensionality from 3 to 1. We compare the nonlinear conductivity with similar zero-density results from the two-particle Boltzmann equation. We also tabulate the variation of the kinetic pressure as a function of the field strength.

KEY WORDS: Gaussian thermostat; two-dimensional, periodic Lorentz gas; hard disks; conductivity; fractal.

1. INTRODUCTION

The simplest known nonequilibrium steady-state problem with reversible equations of motion is the Galton board[1,2] or Lorentz gas problem (Fig. 1). A single point particle of mass m moves with velocity v and momentum $p = mv$ through a regular lattice of fixed scatterers of diameter σ under the influence of two external fields F_d and F_c. An equivalent alter-

[1] Lawrence Livermore National Laboratory, and Department of Applied Science, University of California at Davis-Livermore, Livermore, California 94550.
[2] Institute for Advanced Studies at Palermo, Sicily, Italy.

0022-4715/87/0800-0709$05.00/0

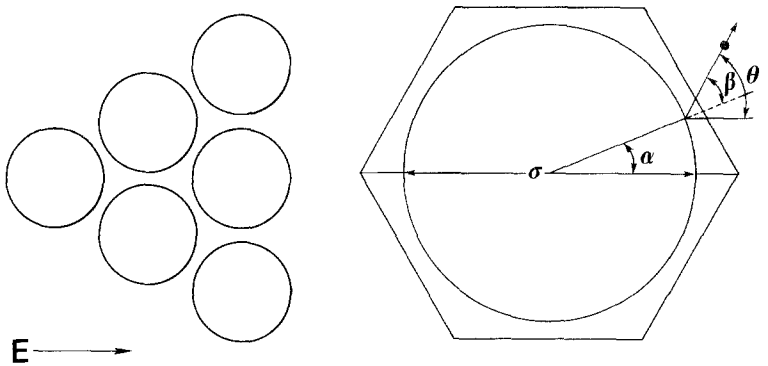

Fig. 1. Geometry of the Lorentz gas. A fixed scatterer particle with diameter σ lies in a hexagonal cell of volume $(3/4)^{1/2}(V/V_0)\sigma^2 = 5V_0/4$, where V_0 is the close-packed volume, $(3/4)^{1/2}\sigma^2$. A point particle with speed v, mass m, and kinetic energy $mv^2/2 = p^2/(2m)$ scatters elastically from the curved surface of the fixed particle. The two angles α and β define a collision, α being measured relative to the field direction and β being measured relative to the normal following the collision.

native view of the dynamics results if *two* identical particles with mass $2m$, diameter $\sigma/2$, velocities $\pm v/2$, and momenta $\pm p$ move with appropriate periodic boundaries. The constant driving field

$$F_d = E$$

generates a net velocity in the field direction. At the same time the time-varying thermostatting or constraining force F_c maintains the system at a constant "temperature" (kinetic energy) and thereby makes a steady state possible:

$$F_c = -\zeta p; \qquad \zeta = E(p_x/m)/(p^2/m)$$

It is necessary to introduce a constraint force in order to observe a steady nonequilibrium state. In the absence of a constraint the thermal velocity p/m, by conservation of the total energy $(p^2/2m) - Ex$, would have to vary as the square root of the x displacement. With growing x displacement the acceleration due to the field, which is independent of velocity, becomes negligible relative to the scattering accelerations, which are proportional to the velocity. In this long-time limit the low-field conductivity, which varies inversely as the velocity for hard disks, might be expected to describe the motion. At long times the drift velocity $\langle dx/dt \rangle$ would then vary as $x^{-1/2}$ and the resulting net displacement varies as the two-thirds power of time. In fact, the motion resulting in the absence of

constraints is so irregular that we could not determine a quantitative power-law dependence of $\langle dx/dt \rangle$ on x.

Thus, a constraint force of some kind must be imposed in order to observe steady diffusion outside the linear regime. The friction coefficient ζ could be based on Nosé mechanics, a modification[2–4] of Hamiltonian mechanics readily applicable to the Galton board. But the resulting phase-space description would become more complex, involving five time-dependent variables $\{x, y, p_x, p_y, \zeta\}$ rather than the simpler set of three required by Gaussian dynamics. The present work is based on the simpler dynamics, Gaussian dynamics, the special case of Nosé–Hoover mechanics in which the relaxation time associated with the frictional thermostatting force $-\zeta p$ approaches zero.

It is certainly not obvious, but it is at least plausible that this system will reach a nonequilibrium state with a nonvanishing current approximately equal to the linear-response-theory prediction worked out by Machta and Zwanzig.[5] But the numerical calculations summarized here show consistency with those earlier results together with topologically interesting behavior at higher field strengths where the mean velocity becomes of the order of the thermal velocity.

The problem reduces to a three-dimensional one, with two coordinates $\{x, y\}$ specifying the location of the scattering particle within a unit cell of the scattering lattice and the third coordinate θ giving the angle corresponding to the direction of motion. This dimensionality can be further reduced from three to two by taking advantage of the integrability of the equations of motion between collisions. Thus, the steady-state probability density in the three-dimensional phase space is simply related to the steady-state two-dimensional probability density for collisions. In Section 2 we describe the equations of motion that constitute the mathematical statement of this problem. The numerical solution is described in Section 3, with some of the analysis relegated to the Appendix. Our conclusions are contained in Section 4.

2. MATHEMATICAL FORMULATION

We use Cartesian space coordinates, locating the moving point particle at x and y with a polar velocity coordinate θ giving the direction of motion relative to the x axis. Thus, the velocity components in the x and y directions are proportional to the cosine and sine of θ, respectively:

$$(v_x, v_y) = (p_x, p_y)/m = v(\cos\theta, \sin\theta) = (p/m)(\cos\theta, \sin\theta)$$

Denoting the driving force or field F_d as the vector $(E, 0)$ parallel to

the x axis and the isokinetic constraint force F_c as $-\zeta p$, we obtain the following first-order equations of motion for the scattering particle:

$$\dot{x} = p_x/m = (p/m)\cos\theta$$
$$\dot{y} = p_y/m = (p/m)\sin\theta$$
$$\dot{p}_x = E + F_x - \zeta p_x$$
$$\dot{p}_y = F_y - \zeta p_y$$
$$\dot{\theta} = -(E/p)\sin\theta$$

Note that the "phase space" in which the motion occurs is only three-dimensional (x, y, and θ) because the kinetic energy is fixed. For more details the closely related references by Hoover[2,6] and Morriss[7] can be consulted.

Figure 1 shows the Galton-board geometry. The triangular lattice can be conveniently broken up into either parallelogram or hexagonal cells. Here we use hexagons. The hexagonal cells have an axis of symmetry provided that the field direction is chosen to lie at any angle $n\pi/6$ relative to a lattice direction. Here we arbitrarily choose the field perpendicular to a row of fixed scatterer particles. Provided that the density of these particles relative to their close-packed density exceeds 3/4, there is no possibility that the moving point particle can avoid scattering. In the present work we arbitrarily choose a density equal to 4/5 the maximum close-packed density. In the Machta–Zwanzig system of units, with scatterers of unit radius separated by a distance $2 + W$, our density choice corresponds to a value for their W of $\sqrt{5} - 2 = 0.236068$.

The equations of motion can be integrated analytically[6] to calculate the displacements Δx and Δy parallel and perpendicular to the field direction during the time t:

$$\Delta x = -(p^2/mE)\ln(\sin\theta/\sin\theta_0)$$
$$\Delta y = -(p^2/mE)(\theta - \theta_0)$$
$$t = -(p/E)\ln[\tan(\theta/2)/\tan(\theta_0/2)]$$

With these results the "collisions" with the horizontal straight-line boundaries of the split-hexagonal cell shown in Fig. 1 can be calculated analytically. A highly accurate calculation of the collisions with the curved disk surface shown in the figure can be based on a rapidly convergent series expansion described in the Appendix. In this way it is possible to treat about 15,000,000 collisions per hour using a Cray-1 computer.

The collision history can then be used to generate either of two

probability density functions, the phase-space density $f(x, y, \theta)$ or the simpler collision probability density $g(\alpha, \beta)$ giving the probability of a collision with configurational angle of impact α and postcollisional direction of motion, relative to head on, described by the angle β. These angles are defined in Fig. 1 and cover the ranges $0 < \alpha < \pi$ and $-\pi/2 < \beta < \pi/2$. For transient problems the full phase-space density f is required. For a steady state the function g is sufficient. This is because the density at any point in phase space can be calculated from the density at the previous collision,

$$f(0)/f(-t) = \exp\left[(E/mv)\int_{-t}^{0} \cos\theta\, dt\right]$$
$$= \exp[E(x(0) - x(-t))/mv^2]$$

or the next collision

$$f(0)/f(t) = \exp\left[(-E/mv)\int_{0}^{t} \cos\theta\, dt\right]$$
$$= \exp[-E(x(t) - x(0))/mv^2]$$

These useful results follow from the analog of Liouville's equation in the three-dimensional phase space:

$$\partial f/\partial t + \partial(f\dot{x})/\partial x + \partial(f\dot{y})/\partial y + \partial(f\dot{\theta})/\partial\theta = 0$$

The various derivatives in the nonequilibrium steady state for x and y in the streaming region between collisions are

$$\partial\dot{x}/\partial x = \partial\dot{y}/\partial y = 0, \qquad \partial\dot{\theta}/\partial\theta = -(E/mv)\cos\theta$$

From these

$$df/dt = \partial f/\partial t + \dot{x}\,\partial f/\partial x + \dot{y}\,\partial f/\partial y + \dot{\theta}\,\partial f/\partial\theta = f(E/mv)\cos\theta$$

which gives directly

$$f(t)/f(0) = \exp(E\,\Delta x/mv^2)$$

The relationship between the probability density in the full space $f(x, y, \theta)$ and the probability density at collisions $g(\alpha, \beta)$ follows from the observation that the collision rate at any angle α is proportional to the velocity component in the radial direction, $(p/m)\cos\beta$. Thus we have

$$f(x = \cos\alpha,\ y = \sin\alpha,\ \theta = \alpha + \beta) = g(\alpha, \beta)/\cos\beta$$

Table I. Conductivity κ as a Function of Field Strength for a Triangular Lattice Lorentz Gas at 4/5 the Close-Packed Density[a]

$Em\sigma/p^2$	$E\tau_0/p$	N	$\kappa p/m\sigma$	$\Gamma m\sigma/p$	$\langle \cos^2\theta \rangle$
0.1	0.030	4×10^7	0.0977	3.365	0.500
0.2	0.059	4×10^7	0.0954	3.364	0.501
0.3	0.089	4×10^7	0.0914	3.367	0.502
0.4	0.119	4×10^7	0.0888	3.370	0.503
0.5	0.149	3×10^7	0.0875	3.375	0.503
0.6	0.178	3×10^7	0.0885	3.380	0.505
0.7	0.208	3×10^7	0.0897	3.388	0.506
0.8	0.238	3×10^7	0.0904	3.392	0.508
0.9	0.267	3×10^7	0.0904	3.391	0.510
1.0	0.297	3×10^7	0.0924	3.394	0.512
1.1	0.327	3×10^7	0.0930	3.397	0.513
1.2	0.357	3×10^7	0.0936	3.398	0.520
1.3	0.386	3×10^7	0.0920	3.396	0.525
1.4	0.416	3×10^7	0.0912	3.406	0.527
1.5	0.446	3×10^7	0.0892	3.409	0.533
1.6	0.475	3×10^7	0.0855	3.412	0.535
1.7	0.505	3×10^7	0.0815	3.419	0.536
1.8	0.535	3×10^7	0.0799	3.434	0.536
1.9	0.565	3×10^7	0.0788	3.446	0.538
2.0	0.594	2×10^6	0.0771	3.456	0.539
2.1	0.624	2×10^6	0.0747	3.474	0.542
2.2	0.654	2×10^6	0.0739	3.495	0.543
2.3	0.683	2×10^6	0.0729	3.512	0.545
2.4	0.713	1×10^6	0.0715	3.536	0.547
2.5	0.743	1×10^6	0.0721	3.550	0.550
2.6	0.773	1×10^6	0.0729	3.561	0.555
2.7	0.802	1×10^6	0.0739	3.554	0.560
2.8	0.832	1×10^6	0.0746	3.559	0.565
2.9	0.862	1×10^6	0.0738	3.561	0.567
3.0	0.891	1×10^6	0.0734	3.554	0.574
3.1	0.921	1×10^6	0.0730	3.550	0.582
3.2	0.951	1×10^6	0.0725	3.544	0.588
3.3	0.981	1×10^6	0.0735	3.542	0.595
3.4	1.010	1×10^6	0.0717	3.522	0.609
3.5	1.040	1×10^6	0.0752	3.525	0.618
4.0	1.189	1×10^6	0.0654	3.396	0.665
4.5	1.337	1×10^6	0.0589	3.192	0.691
5.0	1.486	1×10^6	0.0575	3.159	0.706
5.5	1.634	1×10^6	0.0546	3.067	0.723
6.0	1.783	1×10^6	0.0827	2.562	0.744
6.5	1.931	1×10^6	0.0492	2.808	0.753
7.0	2.080	1×10^6	0.0364	2.892	0.764
7.5	2.228	1×10^6	0.0414	2.976	0.771
8.0	2.377	1×10^6	0.0395	3.124	0.776
8.5	2.526	1×10^6	0.0424	3.137	0.782
9.0	2.674	1×10^6	0.0485	2.704	0.782
9.5	2.823	1×10^6	0.0333	3.084	0.795
10.0	2.971	1×10^6	0.0484	3.000	0.796

[a] N is the number of disk collisions, Γ is the collision rate, and τ_0 is the mean time between successive collisions at zero field. The conductivity is given by the average value of the velocity in the field direction divided by the field strength. In the two-particle view, with velocities $\pm$ half the one-particle value, $\langle v \rangle/E$ would have half the tabulated value.

The steady-state pressure tensor can likewise be expressed in terms of α and β, taking into account that the collisions are isokinetic rather than isoenergetic, as is explained in Refs. 8 and 9. The kinetic contribution to $P_{xx}V(m/p^2) = \langle \cos^2 \theta \rangle$ is given in Table I.

3. NUMERICAL RESULTS VIA NONEQUILIBRIUM MOLECULAR DYNAMICS

Calculations spanning two orders of magnitude in the field strength E are summarized in Table I. The results can be checked in several ways. First, the limiting conductivity at vanishing field strength can be compared with the purely equilibrium calculation of Machta and Zwanzig.[5] Within the 5% uncertainties of the extrapolation and the equilibrium calculations the two approaches agree.

Next, at zero field, the fraction of collisions with the disk is given by the ratio of the half-disk perimeter $\pi\sigma/2$, where σ is the disk diameter to the exposed area of the half hexagon. This value is 0.4136. Because the system is a mixing system, the collision rate Γ can be likewise be calculated

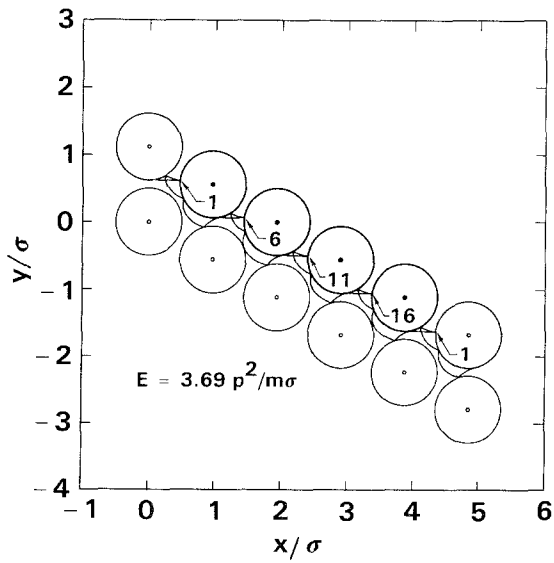

Fig. 2. Cycle of 20 collisions stable at a field strength of $E = 3.69\,p^2/m\sigma$. This pattern corresponds to the 20 spots that develop in the probability density function shown in Fig. 3. Collisions 1, 6, 11, and 16 in the cycle are labeled here and correspond to the rightmost dot in Fig. 3.

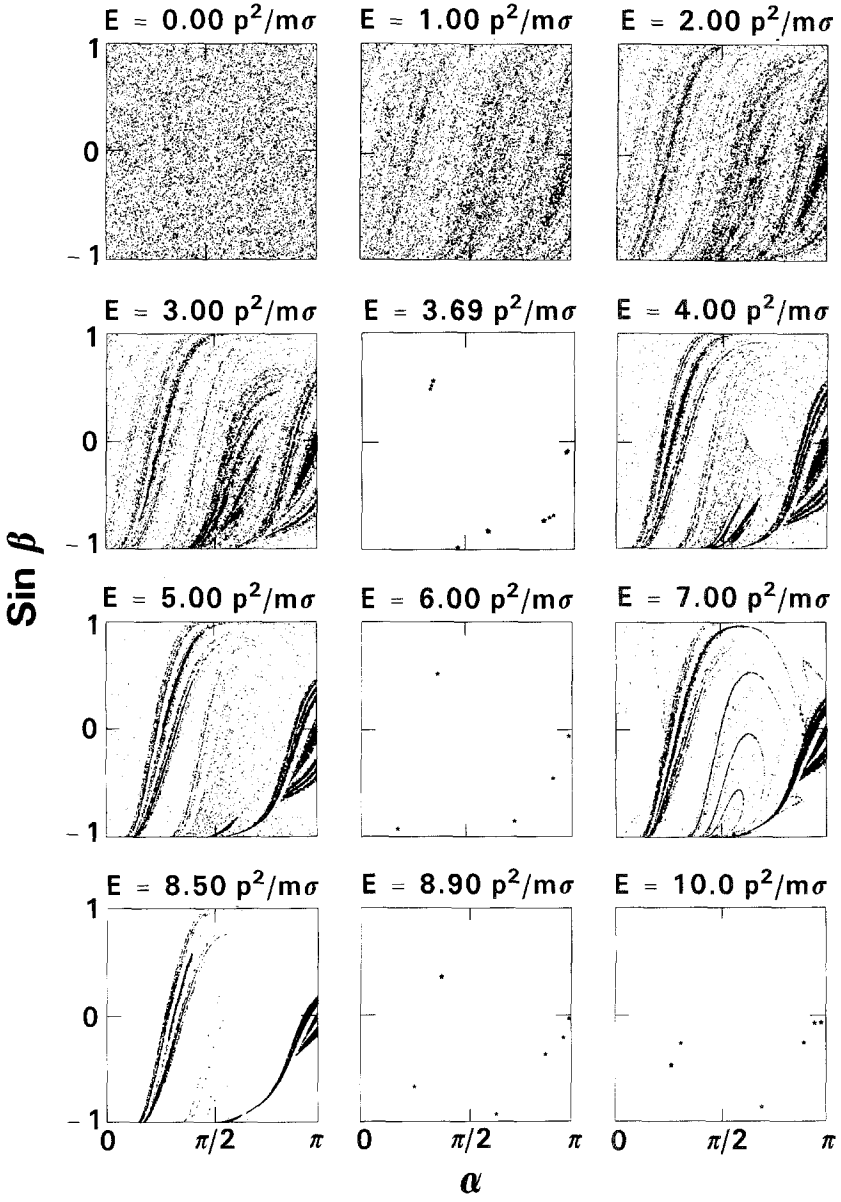

Fig. 3. Field-strength dependence of the probability density $g(\alpha, \beta)/\cos\beta$ with increasing field strength. This density function is unity for zero field and approaches 20 δ-functions (5 clusters of 4) at a field strength of 3.69 $p^2/m\sigma$.

Table II. Limit Cycles of n Collisions Each Found at Field Strength E with the Corresponding Conductivities κ

$Em\sigma/p$	3.69	6.00	6.17	6.56	8.29	8.90	9.05	9.24	9.29	9.47	9.66	9.78	10.0
n	20	5	14	6	8	6	19	8	10	8	32	10	6
$100\kappa p/m\sigma$	13.4	8.27	7.32	6.03	5.64	5.02	5.06	4.20	3.30	3.79	3.93	3.52	4.84

analytically, with the result $3.3655v/\sigma$. Both numerical estimates were reproduced to three-figure accuracy in runs of one million collisions, as would be expected from the central limit theorem.

The probability density g is extremely interesting; it varies from a $\cos\beta$ distribution spanning the two-dimensional α–β space at zero field, to a set of 20 discrete, equally weighted dots at a field of $3.69p^2/m\sigma$. Thus, the dimensionality of the probability density g must vary between two and zero, suggesting "fractal" nonintegral values in between. A fractal object is typically one in which the number of pairs of points lying within a range dr about a point r within the object varies as a nonintegral power of r. We found that this nonintegral power is 1.8 for a field of $2p^2/m\sigma$ and 1.6 for a field of $3.6p^2/m\sigma$. The definitions of various nearly equivalent fractal

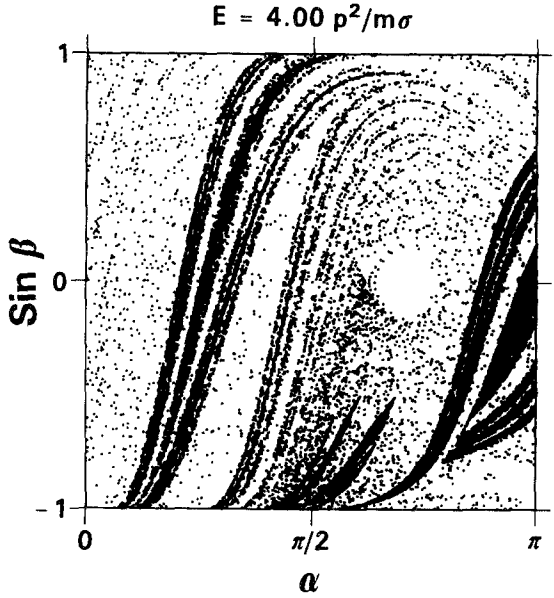

Fig. 4. Enlarged view, with three times as many points, of the "eye" appearing in Fig. 3 with $E = 4p^2/m\sigma$.

dimensionalities together with illustrations suggesting their structure can be found in Refs. 10 and 11. The development of the 20 spots, corresponding to the chain of collisions shown in Fig. 2, can be seen in the series of probability density functions shown in Fig. 3.

We found 13 values of the field strength for which stable collision cycles occur. Those field strengths, the number n of collisions per cycle, and the corresponding conductivities are summarized in Table II.

The "eye" visible just to the right of the center of the $E = 4p^2/m\sigma$ portion of Fig. 3 (see Fig. 4) corresponds to a stable Kolmogorov–Arnold–Moser-like, nearly periodic orbit shown in Fig. 5. It seems likely that more complex nearly periodic orbits occur at other field strengths. Most of the phase space comprises a chaotic region, which, after a few collision times, condenses onto the strange attractors shown in Fig. 3.

Figure 6 shows the dependence of the conductivity κ on field strength. In that figure we scale the results in terms of the collision rate, as was done for the low-density case in Ref. 6. In both cases the conductivity is a generally decreasing function of field strength, but with considerable structure at low fields. The structure is the complicated consequence of the change in relative importance of first-, second-, and third-neighbor collisions as a function of field strength.

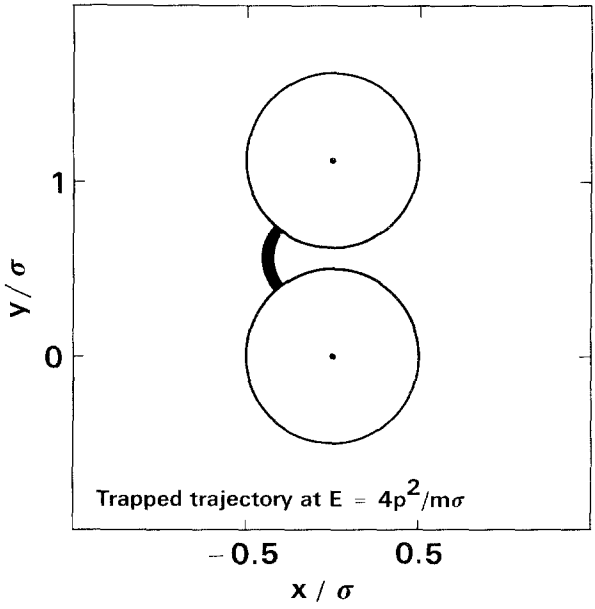

Fig. 5. Trapped trajectory corresponding to the "eye" seen in Figs. 3 and 4 at a field $E = 4p^2/m\sigma$. The motion is quasiperiodic and stable.

Figure 7 shows a different representation of the probability density $g(\alpha, \beta)$ as a coarse-grained surface over a 180×180 grid in α–β space. It is certainly suggested by the figures that the probability density is a fractal.[4,11] If we index the grid with two subscripts i and j, the coarse-grained probability density g_{ij} can be found as the solution of a steady-state matrix equation relating the probability of successive collisions:

$$g_{ij} = M_{ijkl}\, g_{kl}$$

The matrix $M = \{M_{ijkl}\}$ is a sparse "normal" matrix, with elements $\exp(Et/p)$, where t is the time required to stream from the collision specified by i and j to that specified by k and l. The largest such matrix we considered has $180^4 = 1{,}049{,}760{,}000$ distinct matrix elements. The time-reversibility of the equations of motion has the consequence that the "transpose" of the matrix is equal to its inverse:

$$M_{ijkl} \times M_{klij} = \delta_{ik}\delta_{jl}$$

An iterated solution of the $32{,}400 \times 32{,}400$ matrix M, beginning with a uniform g, where g is a 180×180 array, is shown in Fig. 7. This calculation

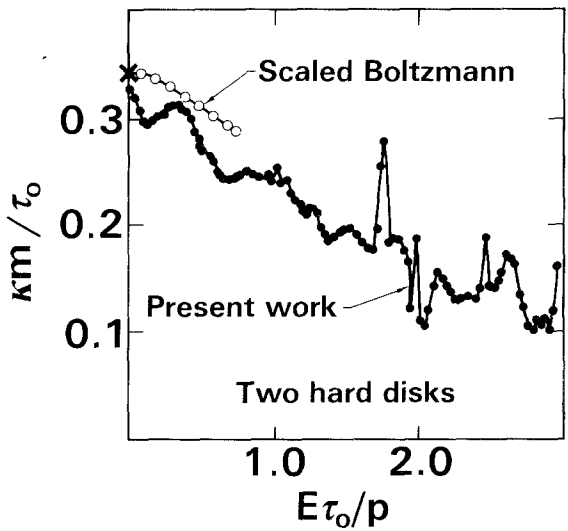

Fig. 6. Nonlinear dependence of conductivity κ (mean velocity divided by field strength) on field strength E. The present work, shown as a series of filled circles, is compared to the low-density Boltzmann-equation results[6] by introducing $\tau_0 = 0.29713 m\sigma/p$, the mean time between successive collisions at zero field. The Boltzmann-equation results are scaled to match the present high-density results ar zero field. ($\times$) Machta and Zwanzig's zero-field conductivity.

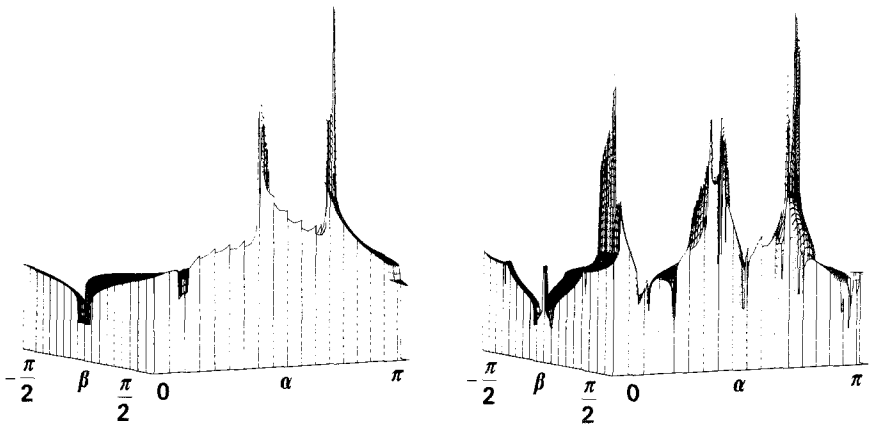

Fig. 7. Representation of the probability density $g(\alpha, \beta)/\cos\beta$ as a surface. The figure compares the first (left) and second (right) approximations based on matrix iteration with a 180×180 grid in α–β space.

required about 1 hr on a CRAY-1. This problem is one on which considerable progress could be made with the development of computers only a few orders of magnitude faster than present machines.

4. CONCLUSIONS

This simple periodic Lorentz gas, or Galton board, equivalent to an isokinetic periodic system of two disks with a driving field, although simple, deterministic, and dynamically time-reversible, displays many of the interesting features of dissipative, irreversible, many-body systems far from equilibrium:

1. *Mixing* in the phase space due to the Liapunov instability[10,12–14] of trajectories—the mixing time is of the order of the time between collisions.
2. *Nonlinear* Conductivity, generally decreasing with increasing field.
3. Complex phase-space geometry, with condensation onto a *strange attractor* with a *fractal* dimensionality.
4. Effective *irreversibility* and *dissipation* with *reversible* equations of motion.

The numerical work has shown that the phase-space probability density has a fractal character, making it extremely unlikely that any efficient analytic description is possible. At the same time, the general dependence of conductivity on field strength is relatively simple, being roughly linear. The details of the dependence are relatively complex.

The reason for the complexity in the phase-space density can be traced to the various kinds of scattering collisions. At the conclusion of a collision, described by the angles α and β, the moving particle can hit any of its six nearest neighbors or any of its six second neighbors. At finite fields even some of the *third* neighbors can be reached—see Fig. 8, where this effect is perceptible for a field strength $E = 0.5p^2/m\sigma$. The types of collisions that occur are shown for 12 field strengths in the figure. These collisions result in relatively complicated probability densities, as shown in Fig. 3. The structure of the boundaries becomes more complex when the curved trajectories induced by a finite field are included. The presence of a field also destroys the rotational symmetry of the scattering as a function of α. The iteration of these boundaries, corresponding to the actual sequence of collisions a particle undergoes, generates a highly complicated structure in the phase space. Because the net motion is primarily in the direction of the field, the volume occupied in the space decreases exponentially in time, thereby establishing that the dimensionality of the probability density is less than that of the space in which it is embedded.

Machta and Zwanzig[5] commented on the very irregular structure they discovered in the velocity autocorrelation function for this same model. That irregular structure no doubt has its origin in the superposition of relatively smooth distributions for particles constrained to collide with particular choices among the neighboring disks available for scattering.

The decrease in occupied phase-space volume is, in the steady state, balanced by continual spreading and bifurcation due to the hard-disk collisions. Thus the phase-space density contraction from the thermostat can be directly related to the compensating Liapunov instability of the trajectories.

In the unstable reversed motion the velocity (or momentum) and the friction coefficient ζ both change sign. Thus, any solution of the equations of motion with a positive conductivity would correspond to a solution with a negative unphysical conductivity in the reversed motion. Because the reversed motion is subject to Liapunov instability and has a relative probability of zero, it cannot actually be observed.

The motion, described in terms of the Liapunov exponents λ_1, λ_2, and λ_3, may seem paradoxical. These exponents[12,13] describe the rate at which a three-dimensional phase-space sphere of points, infinitesimal in radius, deforms into an ellipsoid, with principal axes varying as $\exp(\lambda_i t)$. Directly from the equations of motion, the volume of the sphere must shrink, on the average, so that

$$\lambda_1 + \lambda_2 + \lambda_3 = -(E/p)\langle \cos\theta \rangle < 0$$

On the other hand, the equations of motion are time-reversible, with θ

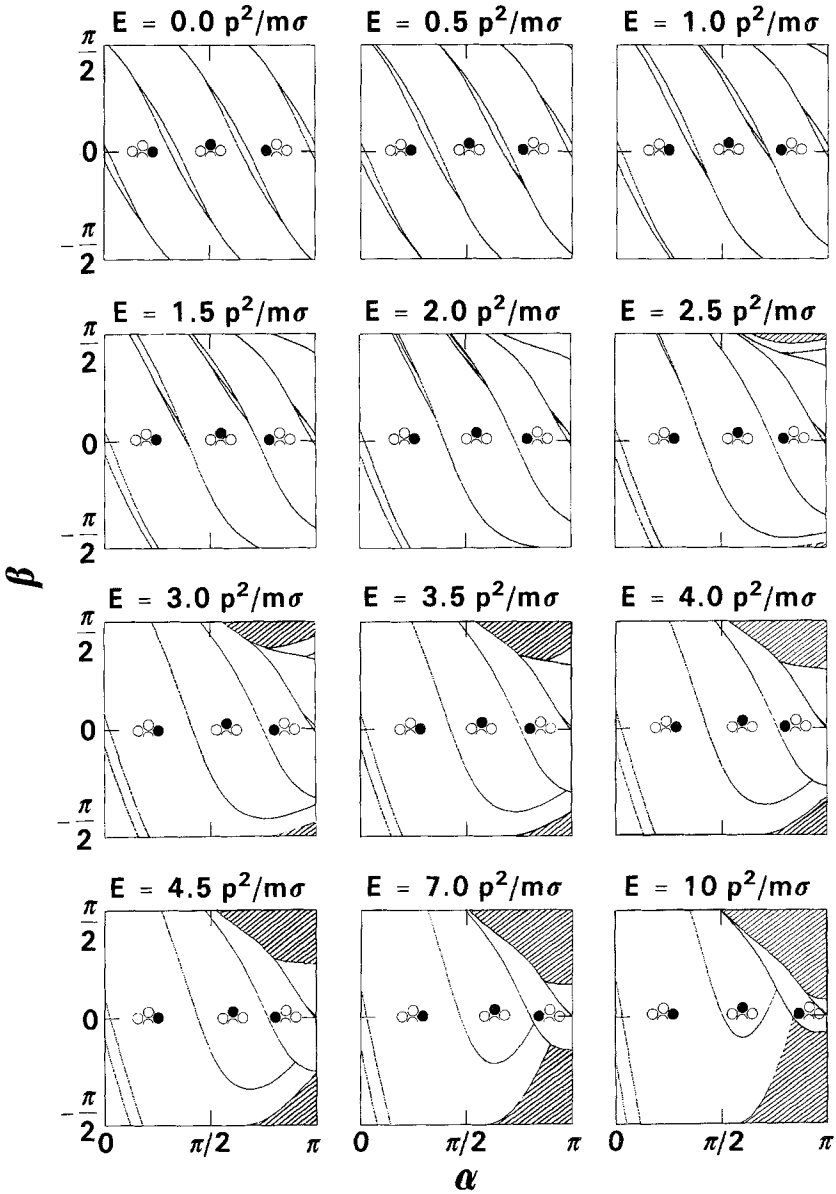

Fig. 8. The regions corresponding to collisions with particular neighbors of the half-disk shown at the bottom of the three sketches. At zero field strength, the boundaries of these regions exhibit threefold symmetry, corresponding to the rotational symmetry of the triangular lattice. This symmetry is lost at finite fields. Iteration of the boundaries results in the fractal structure evident in Figs. 3 and 7. The shaded regions correspond to trajectories starting on the half disk and ending on the same particle. Collisions with the third neighbors at a field of $0.5\,p^2/m\sigma$ form a small, barely perceptible, three-sided region near $\alpha = 3\pi/4$ and $\beta = -\pi/8$. Third-neighbor collisions are more visible at a field of $p^2/m\sigma$ near $\alpha = 3\pi/4$ and $\beta = 0$. Here α and β describe the half-disk postcollision configuration and direction of motion.

becoming $\pi - \theta$ in the reversed motion. In the reversed motion one might expect that the three λ_i would simply change sign, with the results

$$\lambda_1 = -\lambda_3; \qquad \lambda_2 = 0$$

But this is not consistent with the existence of a positive conductivity. What really happens is that the principal directions of growth and decay in the motion are sensitive to initial conditions and differ in the direct and reversed motion. It is unfortunate that a direct measurement of the Liapunov exponents is very difficult for singular potentials, despite the existence of fairly efficient methods for determining these coefficients in simpler problems.[12,13] On the other hand, there are alternative methods for studying the dynamics of constrained systems and it is worthwhile to study their relative merits. Experience with Nosé mechanics[2–4,14] suggests that the Nosé–Hoover formulation for the friction coefficient ζ does little more than complicate the mathematical description, by adding two to the dimensionality of the corresponding phase space.

On the other hand, Lagrangian mechanics[2,14] could be applied to this problem. In that case the Lagrangian has the form

$$L = T(1+\lambda) - \lambda K - \phi$$

where λ is a time-dependent Lagrange multiplier chosen such that the instantaneous kinetic energy $T = mv^2/2$ has the fixed value K. The potential energy ϕ includes both the scattering contributions with the fixed lattice and a linear term $-Ex$ to drive the current. In this Lagrangian case the equations of motion include an effective mass $m(1+\lambda)$ rather than a friction coefficient:

$$p_x = m\dot{x}(1+\lambda), \qquad p_y = m\dot{y}(1+\lambda)$$
$$\dot{p}_x = E + F_x, \qquad \dot{p}_y = F_y$$

where F describes the scattering interaction with the fixed lattice of disks. λ varies with time to ensure that T and K are equal. But it should be noted that in the time-reversed equations of motion λ is unchanged. This suggests that the Lagrangian description is not useful in far-from-equilibrium problems in which nonlinear dissipation must be considered. We have investigated these Lagrangian equations in order to characterize their mode of failure. We found that the parameter λ and the momentum p increase without bound and the corresponding conductivity approaches zero independent of the field strength.

Between collisions the Lagrange equation of $\dot{p}_y$ can be integrated directly:

$$1 + \lambda = [(p_x^2 + p_y^2)/2mK]^{1/2} = \sin\theta_0/\sin\theta$$

where we have arbitrarily chosen to set λ equal to 0 at the initial time, corresponding to a velocity $v(\cos\theta_0, \sin\theta_0)$. From this relation the equation of motion for the angle results:

$$\dot{\theta} = -E\sin^2\theta/\sin\theta_0$$

The equation of motion is identical to the Gaussian version provided that E is sufficiently small so that $\Delta\theta$ can be ignored. For $Em\sigma/p^2 = 1$, 2, and 8, by using the choice $\lambda = 0$ at each collision, we found $\kappa p/m\sigma$ to be 0.098, 0.106, and 0.087.

The linking of successive collisions to the probability density g suggests the formulation of the Galton board problem as a mapping problem, with the collisions corresponding to the iteration process linking g_-, g_o, and g_+. But we have not seen a way to take advantage of this analog. Likewise, the field-driven diffusion problem also bears a qualitative but barren resemblance to a one-dimensional random walk with stochastic collisions.

We wish to add the following comment, responding to one referee's (paraphrased) question, "How seriously should we take isokinetic dynamics?" The need for a systematic approach to dynamical equilibrium was recognized by Einstein,[15] who augmented a frictional force with an irreversible stochastic force to account for the interaction of matter with equilibrium blackbody radiation. A reversible theory of thermal equilibration remains a difficult and desirable goal. Here we are mainly concerned with pointing out generic features (deterministic reversible equations of motion, leading to stable zero-volume attractors with predominantly negative Liapunov exponents) associated with nonequilibrium systems.[16] It is remarkable (as emphasized by the second referee) that even this simple one-body problem reveals profound insight into the generic structure of nonequilibrium distribution functions.

APPENDIX. COLLISIONS WITH THE DISK AND SIDES OF THE HEXAGONAL CELL BASED ON A TAYLOR SERIES EXPANSION IN $\Delta\theta$

The exact trajectory is described in Section 2. The equations of motion can be written as

$$\begin{aligned} x &= x_0 - (p^2/mE)\ln(\sin\theta/\sin\theta_0) \\ y &= y_0 - (p^2/mE)(\theta - \theta_0) \end{aligned} \tag{A1}$$

Expanding around θ_0 in a Taylor series to second order in $\Delta\theta = \theta - \theta_0$, we have

$$\begin{aligned} x &= x_0 - (p^2/mE)[\cot\theta_0\,\Delta\theta - \csc^2\theta_0\,(\Delta\theta^2/2)] \\ y &= y_0 - (p^2/mE)\,\Delta\theta \end{aligned} \tag{A2}$$

Solving to second order the intersection of the trajectory with the disk,

$$\begin{aligned} x^2 + y^2 = \sigma^2/4 \doteq \{x_0 - (p^2/mE)[\cot\theta_0\,\Delta\theta - \csc^2\theta_0\,(\Delta\theta^2/2)]\}^2 \\ + [y_0 - (p^2/mE)\,\Delta\theta]^2 \end{aligned}$$

Keeping terms of order $\Delta\theta^2$ or lower, we have the quadratic equation

$$\begin{aligned} &[(p^2/mE)\csc^2\theta_0\,((p^2/mE) + x_0)]\,\Delta\theta^2 \\ &\quad - [2(p^2/mE)(x_0\cot\theta_0 + y_0)]\,\Delta\theta + (x_0^2 + y_0^2 - (\sigma^2/4)) = 0 \end{aligned}$$

The solution of the quadratic equation gives an approximate value of $\Delta\theta$, which is then used in Eq. (A1) to find an exact point on the trajectory close to the intersection with the disk. The process is repeated to convergence by calculating new coefficients of the quadratic equation. We found that typically, for fields $E \leqslant p^2/m\sigma$, three iterations were sufficient to calculate the coordinates at the intersection to seven significant figures.

To find the intersection with the left and right sides of the hexagonal cell, we note that the equation of the left side is given by the straight line

$$y = 3^{1/2}x + \rho^{-1/2}$$

where ρ is the density relative to the maximum close-packed density. In the calculations described here $\rho = 4/5$.

Solving to second order in $\Delta\theta$ for the intersection with the trajectory, we have

$$\begin{aligned} &[(3/4)^{1/2}\csc^2\theta_0/(p^2/mE)]\,\Delta\theta^2 \\ &\quad + [(1 - 3^{1/2}\cot\theta_0)/(p^2/mE)]\,\Delta\theta + (3^{1/2}x_0 + \rho^{-1/2} - y_0) = 0 \end{aligned}$$

Similarly, for the right side of the hexagonal cell, the straight line is given by

$$y = -3^{1/2}x + \rho^{-1/2}$$

and the quadratic equation becomes

$$\begin{aligned} &[(3/4)^{1/2}\csc^2\theta_0)/(p^2/mE)]\,\Delta\theta^2 \\ &\quad + [(1 + 3^{1/2}\cot\theta_0)/(p^2/mE)]\,\Delta\theta + (3^{1/2}x_0 - \rho^{-1/2} + y_0) = 0 \end{aligned}$$

ACKNOWLEDGMENTS

We thank Bruce Boghosian, Ray Chin, Willy Moss, and J. S. Pack for good advice. S. B. thanks the National Science Foundation for a generous travel grant.

This work was carried out under the auspices of the U. S. Department of Energy at the University of California's Livermore National Laboratory under contract W-7405-Eng-48.

REFERENCES

1. M. Kac, *Sci. Am.* **211**(9):92 (1964).
2. W. G. Hoover, *Molecular Dynamics* (Springer-Verlag, Heidelberg, 1986).
3. S. Nosé, *J. Chem. Phys.* **81**:511 (1984); *Mol. Phys.* **52**:255 (1984).
4. H. A. Posch, W. G. Hoover, and F. J. Vesely, *Phys. Rev. A* **33**:4253 (1986).
5. J. Machta and R. W. Zwanzig, *Phys. Rev. Lett.* **50**:1959 (1983).
6. W. G. Hoover, *J. Stat. Phys.* **42**:587 (1986).
7. G. P. Morriss, *Phys. Lett.* **113A**:269 (1985).
8. W. G. Hoover and K. W. Kratky, *J. Stat. Phys.* **42**:1103 (1986).
9. K. W. Kratky and W. G. Hoover, *J. Stat. Phys.*, to appear (1987).
10. J. D. Farmer, E. Ott, and J. A. Yorke, *Physica* **7D**:153 (1983).
11. B. B. Mandelbrot, *The Fractal Geometry of Nature* (W. H. Freeman, San Francisco, 1982).
12. W. G. Hoover and H. A. Posch, *Phys. Lett.* **113A**:82 (1985).
13. W. G. Hoover, H. A. Posch, B. L. Holian, and S. Bestiale, *Bull. Amer. Phys. Soc.* **32**:824 (1987).
14. W. G. Hoover, *Physica* **118**:111 (1983).
15. A. Einstein, *Z. Phys. Chem.* **18**:121 (1917).
16. W. G. Hoover, B. Moran, B. Holian, H. Posch, and S. Bestiale, in Proceedings of the 5th Topical Conference on Shock Waves in Condensed Matter, Monterey, California, July 1987, *Bull. Am. Phys. Soc.* **32**:1370 (1987).